Calculating radiative corrections for the photon gluon fusion

Fabian Schmidt
H1 group, DESY Zeuthen
Email: fabian.schmidt@physik.hu-berlin.de

This report summarizes the calculation of radiative corrections for charm production in deep-inelastic ep scattering at the HERA collider. These corrections are important for physics analysis at experiments such as H1. The parametrization of the charm structure functions was implemented in the `HECTOR` *program so that* `HECTOR` *now calculates radiative corrections for deep inelastic scattering as well as for photon gluon fusion.*

1 Introduction

1.1 Deep-inelastic scattering

The H1 experiment at the HERA collider at DESY, Hamburg, studies deep inelastic scattering (DIS) of electrons or positrons from protons. Typical beam energies are 27.5 GeV for the electrons or positrons and 920 GeV for the protons. The details about physics at HERA can be found in [1].
The Born-level (leading order) Feynman diagram of DIS is shown in figure 1. The electron and a quark of the proton exchange a virtual boson (γ, Z, or $W^{\pm}$) carrying a 4-momentum $q = p'_e - p_e$. DIS is characterized by a large absolute invariant mass $Q^2 = -q^2$ (at least 1 GeV^2) of the virtual boson. Apart from Q^2, the kinematics of DIS are described by the following variables:

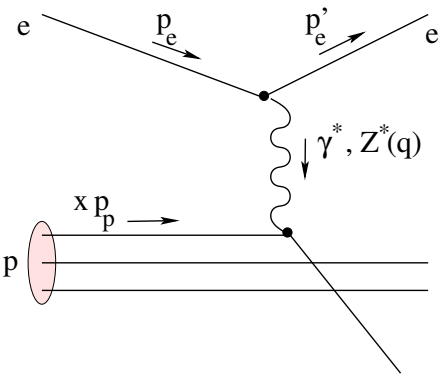

Fig. 1: *Born level diagram of the DIS process.*

$$x = \frac{Q^2}{2\, p_p \cdot q} \quad \text{(Bjorken-x)}$$

$$y = \frac{p_p \cdot q}{p_p \cdot p_e} \quad \text{(inelasticity)}$$

$$W^2 = (p_p + q)^2 = Q^2(\frac{1}{x} - 1) + M_p^2 \quad \text{(invariant mass of the } \gamma^* p \text{ system)}$$

These satisfy the relations $Q^2 = x\, y\, s$ and $W^2 \approx Q^2/x$, where s is the center-of-mass energy squared and M_p is the proton mass. Hence, only three of these kinematical variables are independent.

A distinction is made between the processes $e^{\pm}\, p \to e^{\pm}\, X$ where a γ or Z is exchanged (neutral current, NC) and $e^{\pm}\, p \to \nu(\bar{\nu})\, X$, where the charged bosons $W^{\pm}$ are exchanged (charged current, CC). Here, only the NC process will be considered.

1.2 Structure functions of the proton

Both γ^* and Z exchange as well as the γ/Z interference term contribute to the NC cross section. Because of the propagator factors of $1/M_Z^2$ and $1/M_Z^4$, respectively, in the latter two terms, these are strongly suppressed at the relevant values of Q^2. In the following, therefore, only the pure γ exchange cross section will be regarded.

Using the structure functions F_1 and F_2, the double differential cross section for DIS (e^+p) can be represented as follows:

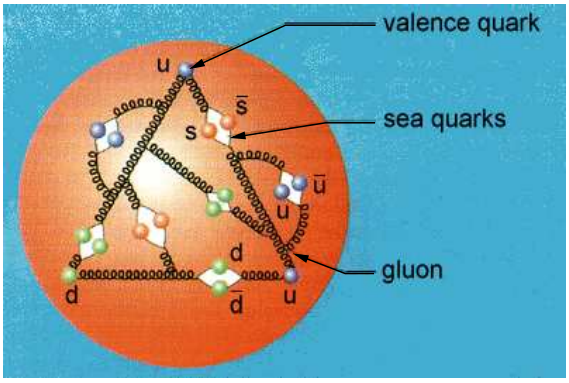

Fig. 2: *An illustration of the proton structure*

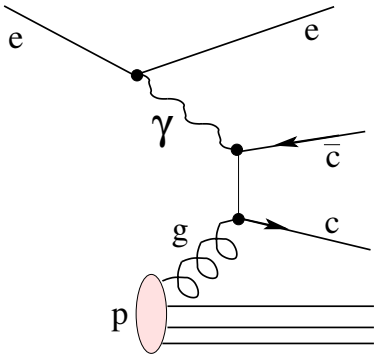

Fig. 3: *Feynman diagram for the charm production by photon gluon fusion*

$$\frac{d^2\sigma}{dx\,dQ^2}(x,Q^2) = \frac{2\pi\alpha^2}{x\,Q^4}(2y^2\,xF_1(x,Q^2) + 2(1-y)F_2(x,Q^2)) \tag{1}$$

where α is the electromagnetic coupling constant.

In the naive quark parton model (QPM, see fig. 2) the proton is considered as a bundle of quarks and gluons (collectively known as partons), with collinear momenta, neglecting masses and transverse momenta of the partons. The Bjorken-x can then be seen as the fraction of the proton momentum carried by the parton involved in the DIS process. In the QPM, F_1 and F_2 can be constructed as follows:

$$F_1(x,Q^2) = \frac{1}{2}\sum_{q=u,d,s} Q_q^2(q(x,Q^2) + \bar{q}(x,Q^2)) \tag{2}$$

$$F_2(x,Q^2) = \sum_{q=u,d,s} x\,Q_q^2(q(x,Q^2) + \bar{q}(x,Q^2)) \tag{3}$$

$u(x,Q^2)$, $d(x,Q^2)$ etc. can be interpreted as quark momentum densities of the u, d etc. quarks and correspondingly for the antiquarks $\bar{u}$, $\bar{d}$, etc. (currently there is no need to assume the existence of heavy sea quarks (c, b, or t) in the proton). Analogously, there is also a gluon density $g(x,Q^2)$; this, however, does not enter the Born level DIS cross section.

In the QPM, F_1 and F_2 satisfy the Callan-Gross-relation $F_T := 2xF_1(x,Q^2) = F_2(x,Q^2)$. The structure function F_T correponds to the transverse cross section where the exchange photon is transverse (helicity ± 1). The longitudinal structure function, corresponding to processes involving longitudinal photons (helicity 0), is defined as $F_L = F_2 - 2xF_1$, so that

$$F_2(x,Q^2) = F_T(x,Q^2) + F_L(x,Q^2).$$

Thus F_L vanishes in the naive QPM.

1.3 Photon gluon fusion

Experimental measurements of the quark densities have shown that the quarks carry only about one half of the proton momentum. Since the gluons should contribute the other half, it is very important to measure the gluon density of the proton. A convenient way of doing this is to use the process of photon gluon fusion (PGF, see fig. 3), as it has a clear experimental signature. In PGF the virtual exchange photon produces a quark-antiquark pair together with a gluon from the proton:

$$\gamma + g \to c\,\bar{c}$$

In the "massive approach" followed here, only three active flavors (u, d, and s) are assumed in the proton. For charm production the PGF is then the dominant process. The $c\bar{c}$ pair fragments into hadrons, mostly $D^{*\pm}$ mesons, which can be reconstructed from their decays.

Similarly to eqn. 1, the charm production cross section can be parametrized as

$$\begin{aligned} \frac{d^2\sigma_{c\bar{c}}}{dx\,dQ^2} &= \frac{2\pi\alpha^2}{x\,Q^4}(2y^2\,xF_1^c(x,Q^2) + 2(1-y)F_2^c(x,Q^2)) \\ &= \frac{2\pi\alpha^2}{x\,Q^4}\{(1+(1-y)^2)\,F_2^c(x,Q^2) - y^2F_L^c(x,Q^2)\} \end{aligned} \tag{4}$$

This is the defining equation for the charm structure functions F_2^c and F_L^c.

2 Parametrization of F_2^c and F_L^c

The theoretical predictions for $F_k^c(k = 2,\ L)$ have been derived in [2] using perturbative quantum chromodynamics (pQCD). In the following, the notation of that publication will be adopted.

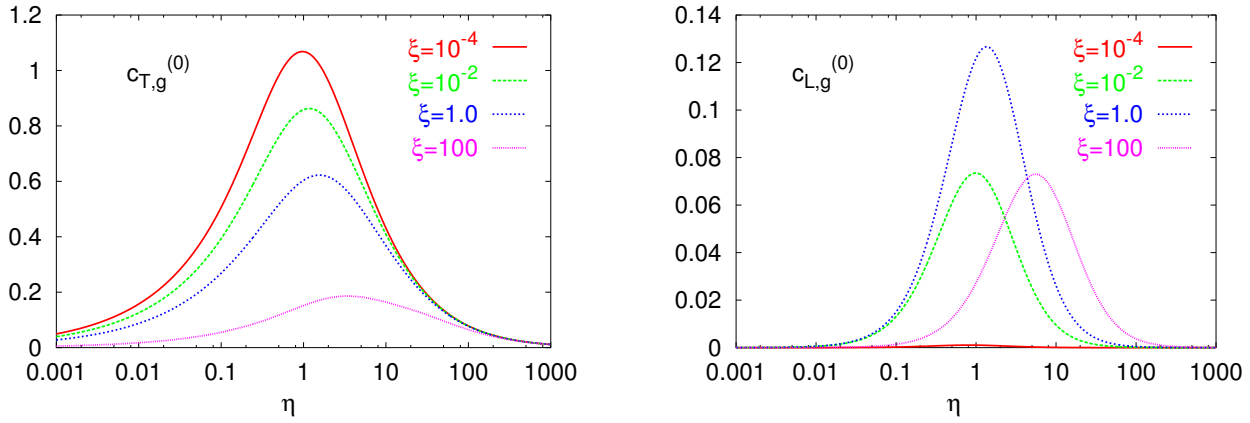

Fig. 4: *The LO transverse (left) and longitudinal (right) coefficient functions for* $F_k^{c(0)}$ *against* η *for different values of* ξ

In leading order (LO, i.e. $O(\alpha_s)$), F_k^c $(k = 2,\ \mathrm{L})$ is determined by the process shown in figure 3 and can be written as follows:

$$F_k^{c(0)}(x,Q^2) = \frac{Q^2\alpha_s}{4\,\pi^2\,m_c^2}\int_x^{z_{max}}\frac{dz}{z}\,e_c^2\,g(x/z,\mu^2)\,c_{k,g}^{(0)} \tag{5}$$

Here, $m_c \approx 1.5$ GeV and $e_c = +2/3$ are the charm quark mass and charge, respectively, and μ^2 is the mass factorization scale which was set to $\mu^2 = Q^2 + 4m_c^2$ in our calculations. The upper integration boundary is $z_{max} = Q^2/(Q^2 + 4m_c^2)$. The quantity $g(x,Q^2)$ denotes the gluon density of the proton, and $c_{k,g}^{(0)}$ $(k = T, L)$, with $c_{2,g}^{(0)} = c_{T,g}^{(0)} + c_{L,g}^{(0)}$, are coefficient functions calculated in [2] in terms of the variables $\eta = s/4m_c^2 - 1$ and $\xi = Q^2/m_c^2$. The LO coefficient functions are shown in figure 4. The transverse coefficient function decreases with growing $Q^2 \propto \xi$, whereas the longitudinal function which is an order of magnitude smaller than $c_{T,g}^{(0)}$, increases up to a certain value of Q^2.

In next-to leading order (NLO, i.e. $O(\alpha_s^2)$), several distinct processes contribute to F_k^c in addition to the LO $F_k^{c(0)}$.

An additional gluon contribution appears due to vertex corrections and the *gluon bremsstrahlung* process:

$$\gamma + g \rightarrow c\,\bar{c} + g$$

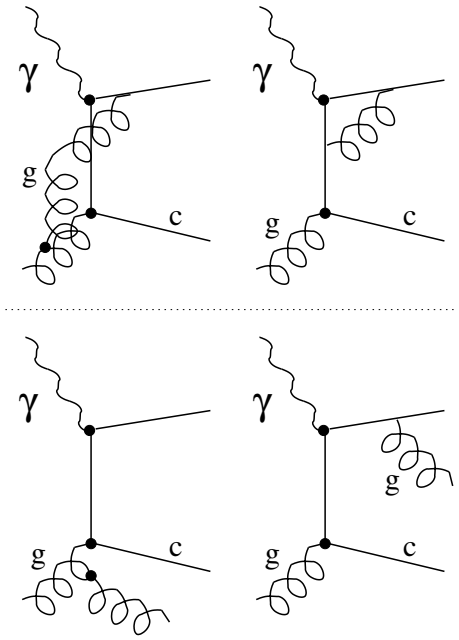

Fig. 5: *Examples of Feynman diagrams for QCD vertex corrections (upper panel) and the gluon bremsstrahlung process (lower panel)*

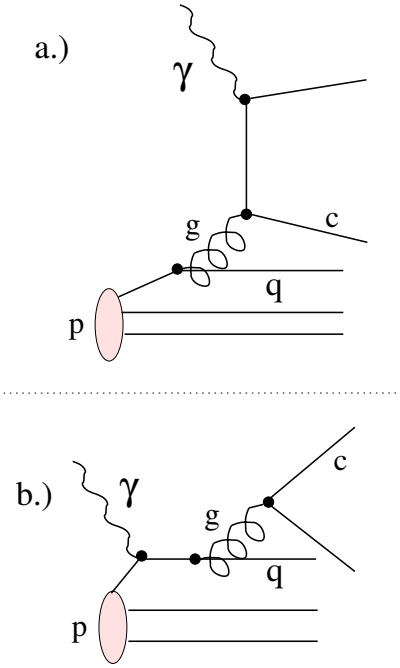

Fig. 6: *Feynman diagrams involving a light quark, correponding to a.) $F_{k,hq}$ and b.) $F_{k,lq}$*

Examples of the relevant Feynman diagrams are shown in figure 5 (there are several more). Similarly to $F_k^{c(0)}$, this contribution, denoted $F_{k,g}^{c(1)}$, is also proportional to the gluon density g:

$$F_{k,g}^{c(1)}(x,Q^2) = \frac{Q^2\alpha_s^2}{\pi\, m^2}\int_x^{z_{max}} \frac{dz}{z}\, e_c^2\, g(x/z,\mu^2)\, (c_{k,g}^{(1)} + \bar{c}_{k,g}^{(1)}\, \ln\frac{\mu^2}{m^2}) \tag{6}$$

Here, a so-called mass factorization part proportional to the logarithm of the factorization scale appears. The corresponding coefficient function is denoted by a bar.

The other two contributions to NLO involve a light quark of the proton (u, d, or s) which emits the participating gluon:

$$\gamma + q \to c\,\bar{c} + q$$

There are two contributions of this type, since the virtual photon can either couple to the charm quark or the light quark (fig. 6), denoted $F_{k,hq}^{c(1)}$ and $F_{k,lq}^{c(1)}$, respectively. Since they involve a sea or a valence quark of the proton, they are proportional to the corresponding quark densities:

$$F_{k,hq}^{c(1)}(x,Q^2) = \frac{Q^2\alpha_s^2}{\pi\, m^2}\int_x^{z_{max}} \frac{dz}{z}\, e_c^2 \cdot \sum_{q=u,d,s} (q(x/z,\mu^2) + \bar{q}(x/z,\mu^2))\, (c_{k,q}^{(1)} + \bar{c}_{k,q}^{(1)}\, \ln\frac{\mu^2}{m^2}) \tag{7}$$

$$F_{k,lq}^{c(1)}(x,Q^2) = \frac{Q^2\alpha_s^2}{\pi\, m^2}\int_x^{z_{max}} \frac{dz}{z} \cdot \sum_{q=u,d,s} e_q^2\, (q(x/z,\mu^2) + \bar{q}(x/z,\mu^2))\, d_{k,q}^{(1)} \tag{8}$$

Because these processes are indistinguishable, their amplitudes have to be summed up before squaring. However, the interference term vanishes after integrating over the internal kinematical variables, so there is no term $\propto e_c\, e_q$. Note that there is no mass factorization part in the $F_{k,lq}$. The coefficient functions $d_{T,q}^{(1)}$ and $d_{L,q}^{(1)}$ (again $d_{2,q}^{(1)} = d_{T,q}^{(1)} + d_{L,q}^{(1)}$) are shown in figure 7. The light quark contribution diminishes with growing Q^2.

Figure 8 shows the different contributions to F_2^c for $Q^2 = 100$ GeV^2. The blue curve shows the absolute value of the sum of the NLO quark contributions, $F_2^{c(1)}(q) = F_{k,hq}^{c(1)} + F_{k,lq}^{c(1)}$, since this sum is negative. The purple curve shows the total NLO F_2^c.

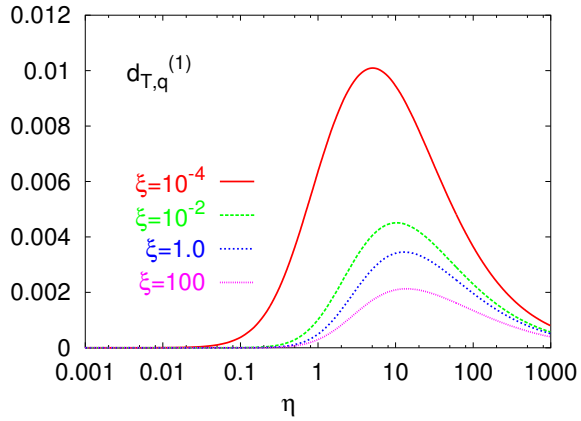

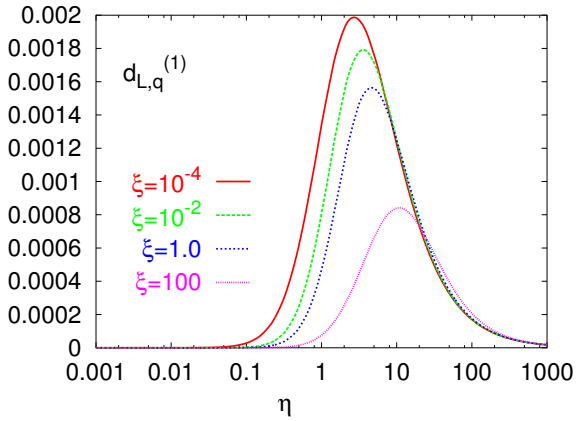

Fig. 7: *The NLO transverse (left) and longitudinal (right) coefficient functions for* $F_{L,lq}^{c(1)}$ *vs.* η *for different values of* ξ

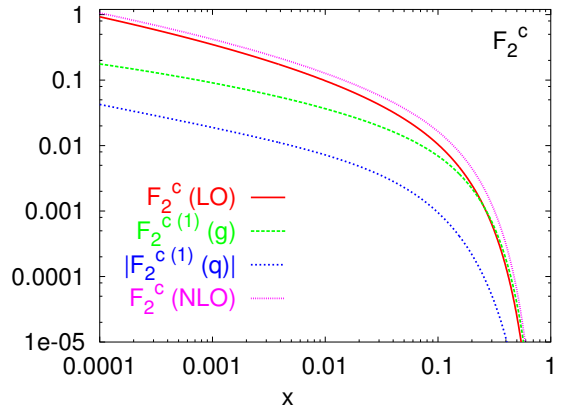

Fig. 8: *The different contributions to* F_2^c *in NLO vs.* x *for* $Q^2 = 100\ \mathrm{GeV}^2$

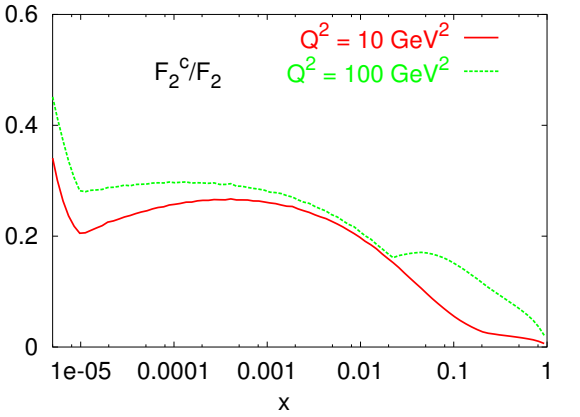

Fig. 9: *The ratio of* F_2^c *to the light flavor structure function* F_2 *vs.* x *at* $Q^2 = 10$ *and* 100 GeV^2

The charm structure functions increase with growing Q^2. In figure 10, $F_2^{c(0)}$ (LO) and $F_2^{c(1)}$ (NLO) are represented against x for Q^2 values of 10 and 100 GeV^2; in figure 11 the same is shown for F_L^c. Note that F_2^c is approximately one order of magnitude larger than F_L^c.

To demonstrate the size of F_2^c in comparison with its light flavor analog F_2, the ratio F_2^c/F_2 is shown as a function of x in figure 9. As expected, the ratio drops for growing x due to the diminishing gluon density for large x. Because of the mass of the charm quarks that have to be produced, the ratio increases with growing Q^2.

In an exact calculation F_k^c should not depend on the factorization scale μ^2. The existing dependence is shown in figure 12 for F_2^c, where the LO and NLO calculations are plotted with μ^2 varying by a factor of 10. It should be noted that the NLO F_2^c depends much less on the value of μ^2 than the LO calculation, as one would expect.

3 Radiative corrections

In addition to the Born level cross section described by the structure functions, radiative and higher order corrections, sometimes collectively known as radiative corrections, have to be accounted for to explain experimental measurements.

In quantum electrodynamics (QED) charged particles continuously radiate photons (fig. 13 a.) and b.)). The radiative corrections accounting for this are very important. If the electron radiates a photon before the interaction, it loses some energy. Then the leptonic Q^2 as determined in the experiment is *not* the momentum

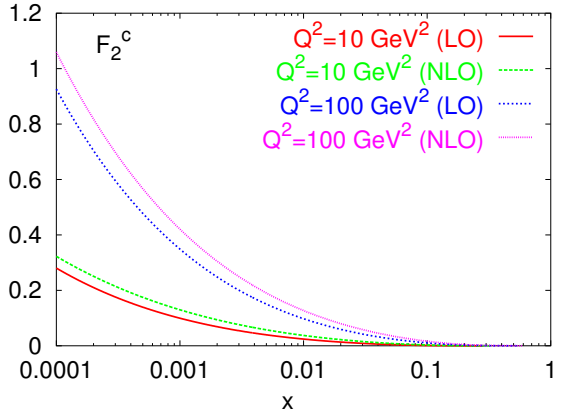

Fig. 10: F_2^c *in leading and next-to leading order vs. x for* $Q^2 = 10, 100\ \mathrm{GeV}^2$

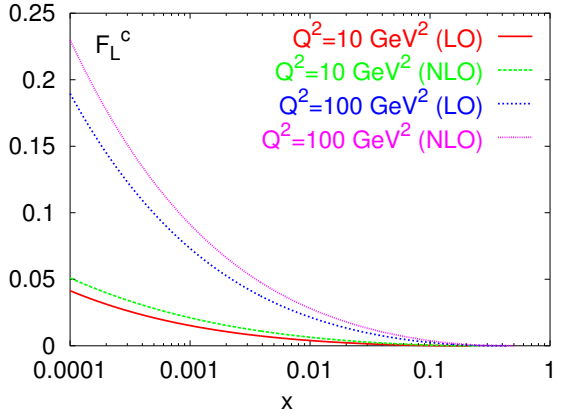

Fig. 11: F_L^c *in leading and next-to leading order vs. x for* $Q^2 = 10, 100\ \mathrm{GeV}^2$

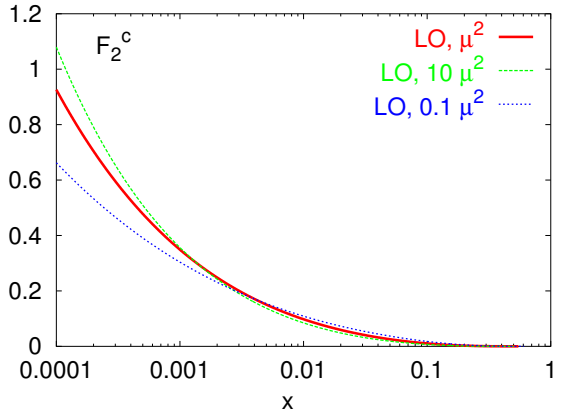

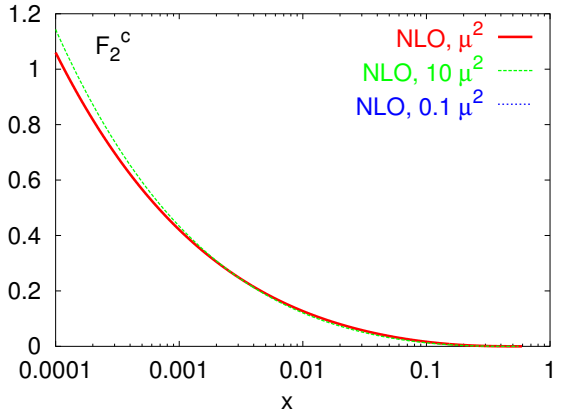

Fig. 12: F_2^c *in LO (left) and NLO (right) for different mass factorization scales:* $\mu^2 = 4m_c^2 + Q^2$, $0.1\ \mu^2$, *and* $10\ \mu^2$

squared (q^2) carried by the exchange photon. $-q^2$ can range from zero up to the leptonic Q^2, resulting in convolution integrals with splitting functions in the calculation of radiative corrections (see [5]).

Higher order corrections involve additional virtual photons or other particles. An important example are the electron vertex corrections (fig. 13 c.)).

A standard technique to obtain the dominant radiative and higher order corrections of QED is the leading-log approximation (LLA). In this approach the terms proportional to $\ln(Q^2/m_e^2)$ which correspond to the collinear mass singularities are separated. Because of the very small mass of the electron, the leptonic corrections are dominant and the radiative corrections of the quarks are often neglected.

The LLA differential cross section can be split into several contributions (in contrast to a full $O(\alpha)$ calculation where this is not possible):

$$\frac{d^2\sigma_{RC}}{dx\,dQ^2}(LLA) = \frac{d^2\sigma^{ISR}}{dx\,dQ^2} + \frac{d^2\sigma^{initial,HO}}{dx\,dQ^2} + \frac{d^2\sigma^{FSR}}{dx\,dQ^2} + \frac{d^2\sigma^{Comp}}{dx\,dQ^2} + \frac{d^2\sigma^{ISR,e^+\to e^-}}{dx\,dQ^2} \tag{9}$$

The first term correponds to initial state radiation (ISR, fig. 13 a.)), the second term comprises the relevant higher order terms from the initial state. It contains non-negligible $O(\alpha^2)$ (2 loop) contributions such as the QED vertex correction (fig. 13 c.)) as well as higher order soft photon contributions. In the case of a neutral current interaction, there is also final state radiation (FSR, fig. 13 b.)), which is calculated in $O(\alpha)$. The next term represents the Compton contribution. This parametrizes the Compton scattering of the positron from the virtual photon "cloud" around the proton in a certain kinematical range. Finally, if the charge of the final state lepton cannot be reconstructed, there is also a $e^+ \to e^-$ conversion term.

Apart from LLA which can be performed to second order, the full $O(\alpha)$ corrections can also be calculated. Then the corrections cannot be split into different terms of ISR, FSR, Compton etc.. Higher order corrections however can only be calculated in the LLA approach.

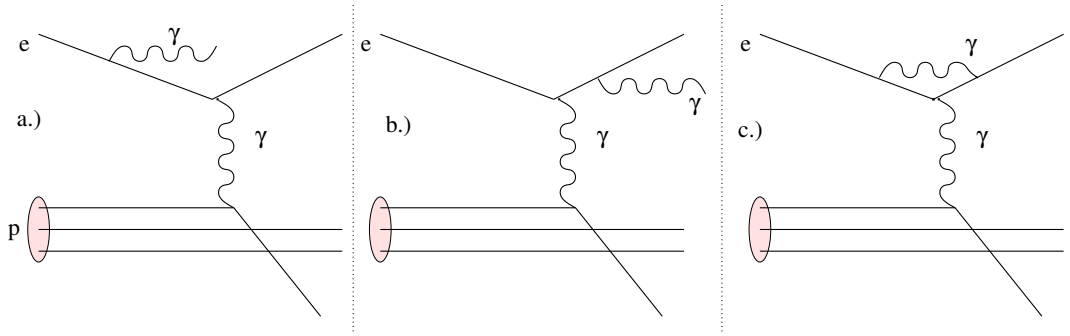

Fig. 13: *The $O(\alpha)$ leptonic QED corrections for DIS, similarly for PGF. The diagrams correspond to a.) ISR b.) FSR, and c.) leptonic vertex correction*

4 Numerical computation of radiative corrections

4.1 The HECTOR *program*

The formulae for the LLA or full $O(\alpha)$ calculation of radiative corrections ([4], [5]) involve integrals that have to be solved numerically. The HECTOR program [4] written in FORTRAN calculates the radiative corrections for deep inelastic scattering according to these approaches for a variety of different kinematical variables. HECTOR has two main branches, named HELIOS and TERAD. HELIOS calculates the corrections in the LLA approach, whereas TERAD computes full $O(\alpha)$ corrections, at the cost of considerably greater run times. HECTOR allows for certain cuts in kinematical variables to better suit experimental requirements (see results section).

It is also possible to calculate hadronic radiative corrections with HECTOR, this, however, was not used in the described calculations.

The program is controlled by numerous flags set in an input file (see [4]). HECTOR prints out the Born cross sections, the corrected cross sections and the relative difference δ between these in bins of two variables. The variables (for example x, y, or Q^2) as well as the bins can be specified by the user. All calculated cross sections are double differential cross sections with respect to the specified variables.

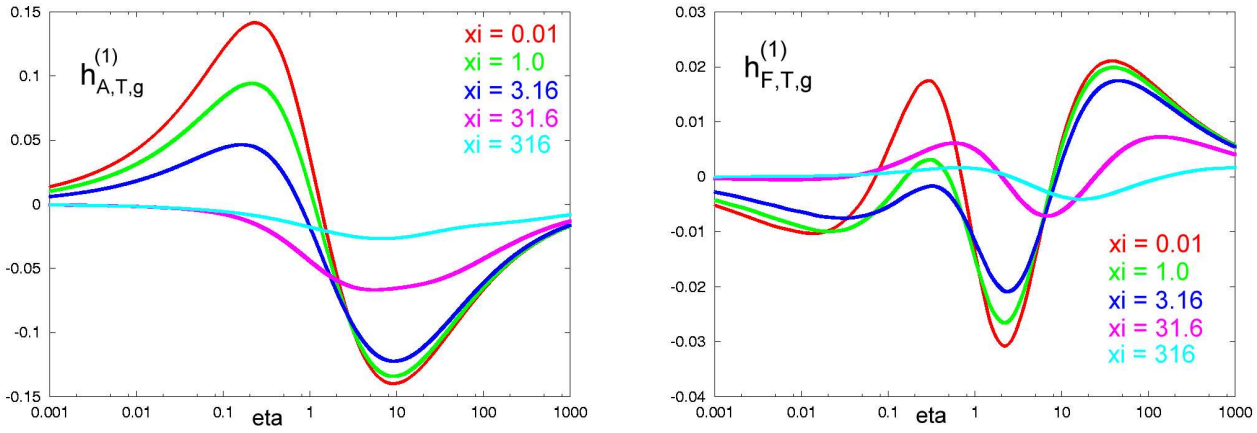

Fig. 14: *The tabulated functions $h^{(1)}_{A,T,g}$ (left) and $h^{(1)}_{F,T,g}$ (right) against η for different values of ξ.*

4.2 Calculating F_2^c and F_L^c

To calculate $F_k^c(k = 2, L)$, the coefficient functions and the parton densities are needed (see eqn. 5 and following). The coefficient functions for the LO F_k^c are given analytically [3], whereas the expressions for NLO are much too lengthy to be published. They are available in tables and can be accessed by an interpolation function for the numerical integration.

Tabulated in $\eta = s/4m_c^2 - 1$ and $\xi = Q^2/m_c^2$ are the coefficent functions separated from their threshold and asymptotic parts. For the latter there are relatively compact analytical expressions. In the case of the NLO gluon contribution, the corresponding tabulated functions, separated into longitudinal and transverse parts, are called $h^{(1)}_{A,k,g}$ and $h^{(1)}_{F,k,g}(k = T, L)$, respectively. A and F stand for different color parts. The transverse functions are shown in figure 14 as functions of η for different values of ξ.

As can be seen by comparing these figures to those in [3], we are using a refined grid (by Andreas Vogt) of the tabulated functions resulting in much smoother plots. Since in this process the notation and normalization of different quantities have been changed in the code, careful testing and recalculation was needed to ensure that the F_k^c computation is correct (the existing program only calculates the coefficient functions, not F_k^c).

First, every coefficient function in LO and NLO was compared to the publication [2] which uses the same notation as [3]. After this comparison it was clear what had been changed during the improvement of the program (e.g. there was a factor of ξ/π added in LO). The new version of the program now follows the notation of [5] rather than that of the original authors. Next, the relation between the two notations had to be established to derive the correct way of calculating F_k^c from the given coefficent functions.

To test the F_k^c code, the integrals were evaluated using 'toy' parton densities, simple analytic expressions without Q^2 evolution, and compared to the results Andreas Vogt obtained with his program. After the agreement of the programs' output had been confirmed, 'real' parton densities could be inserted for the F_k^c calculations.

The parton densities are also available in tables from different sources. They are derived from experimental data under certain theoretical assumptions, using LO or NLO calculations. For all plots shown here except figure 9, the GRV98 parton distributions [6] were used. Figure 9 was generated with the CTEQ 5M1 parton distributions.

An iterative numerical integration routine (`DAIND`) is used to integrate the product of coefficient functions and parton densities.

4.3 Radiative corrections to PGF

To calculate radiative corrections for the photon gluon fusion with `HECTOR`, the program has to be modified since it was originally developed for DIS corrections. Because of the similar definitions of F_k and F_k^c (eqn. 1 and 4), only the ordinary structure functions have to be replaced by the corresponding F_k^c functions.

To keep the program package flexible, two `HECTOR` flags were added, `ICHARM` and `IGLUON`. `ICHARM` controls whether radiative corrections are to be calculated for DIS or for charm production, `IGLUON` sets the gluon density parametrization to be used for the F_k^c calculation. Although not relevant for our calculations, the G_k^c and H_k^c structure functions which describe the γ/Z interference and pure Z term of the NC cross section, are also calculated in the modified `HECTOR` program.

In addition, the `HECTOR` output was extended. `HECTOR` now also prints out the values of the different structure functions for the corresponding values of x and y, or x and Q^2. Of course this is not necessary for the radiative corrections, but it is helpful for diagnostics and may give hints for unreasonable results.

Not surprisingly, the much greater complexity of the calculation of F_k^c compared to that of the 'ordinary' F_k makes `HECTOR` much more time-consuming (by a factor of 800 to 900).

5 Results

All `HECTOR` calculations were performed for an e^+p scattering process with a positron energy of 27.5 GeV and a proton energy of 920 GeV. The variables used are the leptonic variables Q^2, x, y, ... as described in the introduction.

5.1 *Comparison of* TERAD *and* HELIOS *results*

To estimate the deviation of the LLA results from the very time-consuming full $O(\alpha)$ calculations, radiative corrections for charm production by PGF were calculated with three different configurations of HECTOR for three values of x (10^{-4}, 0.1, 0.5) and 100 values of $y \in [0.01, 0.95]$ each.

The settings common to all configurations are :

- inclusion of initial and final state radiation and Compton contribution
- all contributions to NC reaction (γ, Z, and γ/Z interference)
- no $e^+ \to e^-$ conversion
- no electroweak form factors (use of $\sin^2\theta_W^{eff}$)
- no hadronic radiative corrections
- no cuts in kinematical variables

The three configurations, given names for convenient reference, are

HELIOS1: $O(\alpha L)$ LLA calculation without soft photon exponentiation

HELIOS2: $O(\alpha L)$ and $O((\alpha L)^2)$ corrections summed up with HELIOS soft photon exponentiation

TERAD: Full $O(\alpha)$ calculation with higher order corrections from the LLA approach and HELIOS soft photon exponentation.

The last configuration is the most time-consuming since TERAD and HELIOS calculations are combined.
The main HECTOR result is the relative difference of the corrected and Born differential cross sections,

$$\delta = \frac{\frac{d^2}{dxdy}\sigma_B - \frac{d^2}{dxdy}\sigma_{Corr}}{\frac{d^2}{dxdy}\sigma_B},$$

in other words the size of the radiative corrections in relation to the Born cross section. This is also the relevant quantity for the experimental results (see below).

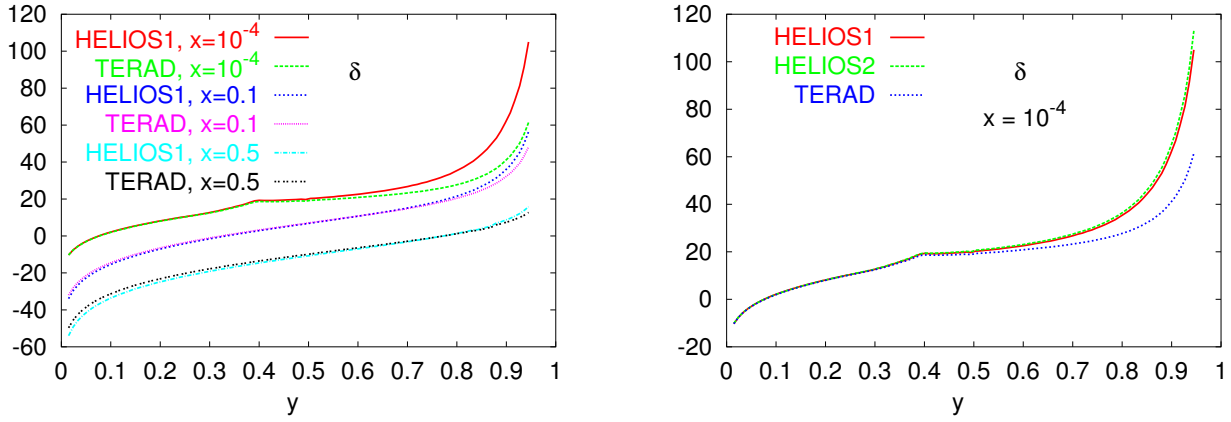

Fig. 15: *The relative size of the radiative corrections, δ (in percent), vs. y; results from the configurations* HELIOS1 *and* TERAD2 *for different x (left), and from the three different configurations and a fixed value of $x = 10^{-4}$ (right).*

In figure 15, δ (in percent) is shown vs. y for the different values of x and the different configurations. The bend in the curves at $y \approx 0.4$ is due to the low Q^2 damping applied to the structure functions in HECTOR to ensure the right $Q^2 \to 0$ behavior. Note that the radiative corrections quickly reach considerable values when y approaches 1. The corrections also fall with growing x (see also fig. 16).

The deviations of the LLA calculations from the full $O(\alpha)$ results also rapidly increase in this region, whereas at $y \lesssim 0.5$ they are negligible. Obviously the LLA estimates are too large at high y values.

The deviations also diminish for growing x. At $x = 0.5$ they are less than 5 % at all values of y. Thus, depending on the kinematical region one is interested in and on one's demands for accuracy, it is often sufficient to use the much faster `HELIOS` branch of `HECTOR`. At large y and small x, however, running `TERAD` becomes inevitable.

5.2 Radiative corrections for H1 kinematics

Radiative corrections are calculated to correct Monte Carlo data, which are generated without incorporating these processes. They have to be computed for those bins in two variables which are also used in the analysis of the experimental data. At H1, a grid in x and y of 32 points each is used. The δ values for this grid are shown in figure 16. They were generated using the `HELIOS1` configuration.

Because of the limited resolution and acceptance of detectors, certain kinematical cuts have to be made when calculating radiative corrections. For example, if events are selected where the charm system has been detected, it has to have at least a certain threshold energy determined by the calorimeter. The `HELIOS` branch of `HECTOR` allows some kinematical cuts to be set. The cuts used for this calculation were a hadronic Q_h^2 of at least 1 GeV^2, a hadronic invariant mass squared of $W_h^2 > 3600\,\text{GeV}^2$, and a $E - p_z$ cut of 40 GeV.

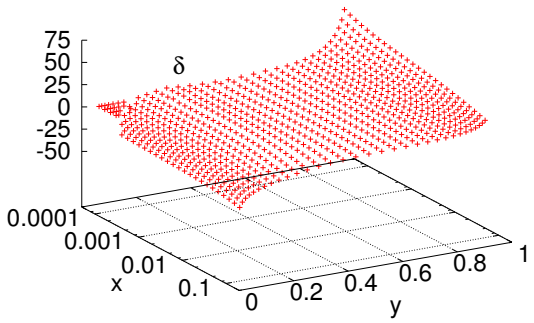

Fig. 16: $\delta(x, y)$ *(in percent) vs. x and y, calculated for the H1 grid.*

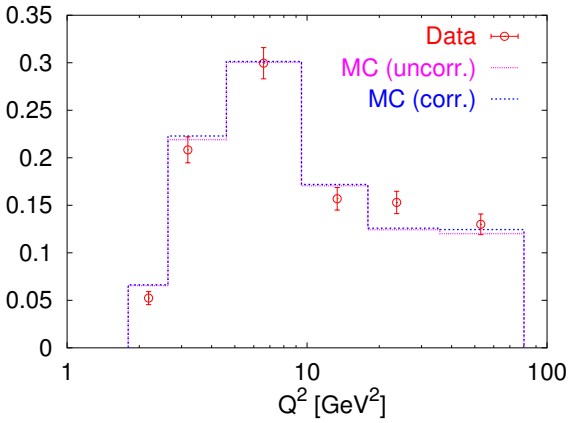

Fig. 17: *Uncorrected and radiative corrected Q^2 distribution of Monte Carlo (MC) generated charm events in arbitrary units. Experimental data points from H1 are also shown.*

From the definition of δ it is obvious how to calculate the corrected cross sections:

$$\frac{d^2\sigma_{Corr}}{dx\,dy} = (1+\delta)\frac{d^2\sigma_B}{dx\,dy}$$

This holds also when using other variables, such as x and Q^2, as long as the bins are transformed properly.

In figure 17, the normalized number of Monte Carlo simulated D^* mesons produced in PGF ($c \to D^* \to D^0 + \pi$) and reconstructed in the H1 detector is shown in bins of Q^2. The simulation was done disregarding any radiative processes; therefore, the uncorrected histogram in figure 17 represents the Q^2 behavior of the Born cross section. Radiative corrections for this Q^2 binning were calculated with `HECTOR` and, interpolating between the bin boundaries, applied to the Born-level distribution. In the same figure, experimental data collected with the H1 experiment (a fraction of the 2000 data production) is shown. The distributions of both simulated and experimental data are normalized to 1. The values of the radiative corrections in figure 17 do not exceed 2 %, for presentation reasons they have therefore been multiplied by a factor of 2.

When calculating double differential cross sections also binned in x, however, the radiative corrections reach considerable values.

Acknowledgements

First of all I would like to thank my supervisor in the summer student program, Katherina Lipka, who was always extremely helpful and accessible. I am also grateful to J. Blümlein for taking the time to answer numerous questions on the theoretical calculation of F_k^c and pQCD in general.

Many thanks of course also go to DESY, and DESY Zeuthen especially, for running the summer student program.

References

[1] HERA brochure published by DESY, Hamburg (2003). Also available at: http://www.desy.de/pr-info/desyhome/gfx/pdf/Broschueren/HERA_en.pdf

[2] E. Laenen, S. Riemersma, J. Smith and W. L. van Neerven, *Nucl. Phys.* B **392**, 162 (1993).

[3] S. Riemersma, J. Smith and W. L. van Neerven, *Phys. Lett.* B **347**, 143 (1995) [arXiv:hep-ph/9411431].

[4] A. Arbuzov, D. Bardin, J. Blümlein, L. Kalinovskaya, T. Riemann, *Comput. Phys. Commun.* **94**, 128-184 (1996).

[5] J. Blümlein, arXiv:hep-ph/9512272 (1995).

[6] GRV98 parton distributions: http://durpdg.dur.ac.uk/hepdata/grv.html, [arXiv:hep-ph/9806404] (1998).